Available online at www.sciencedirect.com
ScienceDirect
International Journal of Heat and Mass Transfer 50 (2007) 1035–1048
International Journal of HEAT and MASS TRANSFER
www.elsevier.com/locate/ijhmt

Extended Shvab–Zel'dovich formulation for multicomponent-fuel diffusion flames

Fernando F. Fachini *

Instituto Nacional de Pesquisas Espaciais, Rod. Presidente Dutra Km 40, 12630-000 Cachoeira Paulista, SP, Brazil

Received 24 February 2005
Available online 1 November 2006

Abstract

In this paper an extension of the Shvab–Zel'dovich formulation is presented. This extended formulation, based on the Burke–Schumann kinetic mechanism, describes the combustion of multicomponent fuels in a diffusion flame in terms of mixture fraction and the excess enthalpy. Under the condition of Burke–Schumann kinetic mechanism, the multicomponent fuel is burned in a single flame. The model is applied to a diffusion flame generated by the burning of mixtures of *n*-heptane and hydrogen diluted in nitrogen in a counterflow configuration. Due to the very small ratio of the hydrogen molecular weight to the *n*-heptane molecular weight, small quantities of hydrogen (in terms of mass) in the mixture does not change significantly the properties related to the mass, like as the total heat released per unit of mass at the flame. However, properties related to the hydrogen mole fraction does change expressively with small quantities, like as the radiative energy loss from the hot region around the flame. The results show the flame properties as a function of the reciprocal scalar dissipation and hydrogen quantity in the mixture. It is observed that, by reducing the reciprocal scalar dissipation, the radiative energy loss decreases and by increasing the presence of the hydrogen, the sensitivity of the flame properties with the reciprocal scalar dissipation reduces. It is also revealed by the results, the effects of the potentiated preferential hydrogen mass diffusion in compositions in which nitrogen and *n*-heptane are the majority species, and the potentiated preferential *n*-heptane thermal diffusion in compositions in which nitrogen and hydrogen are the majority species, on the flame properties. Although, this work do not treat the extinction problem, the fluid dynamical results will be properly handled to provide information about the reciprocal scalar dissipation and the Liñán's parameter necessary for future flame stability analyses.

Keywords: Diffusion flames; Shvab–Zel'dovich formulation; Multicomponent fuel

1. Introduction

This analysis addresses fluid dynamical aspects of the burning of multicomponent fuels in diffusion flame. For that, it is considering the Burke–Schumann kinetic mechanism, which guarantees that the reaction zone of each fuel reaction is inside a single flame.

The infinite reaction rate of the Burke–Schumann mechanism imposes conditions that all reactions take place inside an infinitely thin flame. A question arises when the reactions rates are considered finite. Does the burning of multicomponent-fuels occur in a single diffusion flame?

Hamins and Seshadri [1,2] studied experimentally burning of mixtures of methanol and heptane, methanol and toluene, and methanol, heptane and toluene in a pool configuration with the oxidant flow directed against the liquid surface. They found that the presence of the methanol increases the reactivity of the solutions [1], which permitted the flame to be stable for lower flame temperature values. Also, they observed that, even for finite reaction rate, for some mixtures, the fuels go to zero practically in the same place inside the flame. However, for other mixtures, the fuels do not vanish at the same place, but the structure of the flame described by the intermediate species did not point out two separate reaction zones. Therefore, the assumption of single flame for multicomponent fuels is valid even for the analysed cases with finite reaction rate.

* Tel.: +55 12 3186 9268; fax: +55 12 3101 1992.
E-mail address: fachini@lcp.inpe.br

0017-9310/$ - see front matter © 2006 Elsevier Ltd. All rights reserved.
doi:10.1016/j.ijheatmasstransfer.2006.07.036

Nomenclature

B_i	frequency factor for reaction i
$\tilde{c}_i$	stoichiometric coefficient (massic) of CO_2 for reaction i
c_p	specific heat at constant pressure
d_i	$\equiv \mathrm{d}y_i/\mathrm{d}x\|_{x=x_f}$
d_θ	$\equiv \mathrm{d}\theta/\mathrm{d}x\|_{x=x_f}$
Da	Damköhler number
D_i	diffusion coefficient for species i
E_i	activation energy
$\tilde{h}_i$	stoichiometric coefficient (massic) of H_2O for reaction i
H	excess enthalpy
J	constant
k	thermal conductivity
l	distance between nozzles
l_P	Planck-mean absorption length
$L(Z)$	function of Z
Le	generic Lewis number
$N(Z)$	function of Z
p	pressure
P	nondimensional pressure
Pe	Peclet number
Pr	Prandtl number
q_{rd}	radiative energy
Q_i	heat released by the reaction i
q_i	$\equiv Q_i Y_{O0}/(c_p T_0 s_i Le_O)$ nondimensional heat released
r	$\equiv r/l$ nondimensional radial coordinate
s_i	stoichiometric coefficient (massic) of O_2 for reaction i
S_H	source term of the H equation
S_Z	source term of the Z equation
T	temperature
u	radial component of the velocity
U	$\equiv u/v_0$ nondimensional radial velocity
v	axial component of the velocity
V	$\equiv \rho v/\rho_0 v_0$ nondimensional axial momentum
x	$\equiv x/l$ nondimensional axial coordinate
X_i	mole fraction for species i
y_i	$\equiv Le_O s_i Y_i / Y_{O0} Le_i$ re-scaled mass fraction
Y_i	mass fraction for species i
Z	mixture fraction
$\beta_{i\bullet}$	global reaction order
γ	relative difference of the heat fluxes
θ	$\equiv T/T_0$ nondimensional temperature
μ	coefficient of viscosity
ρ	density
ϱ	$\equiv \rho/\rho_0$ nondimensional density
σ	Stefan–Boltzmann constant
χ_f	scalar dissipation
ω_i	rate for reaction i

Subscripts

0	boundary condition at the air nozzle
1	boundary condition at the fuel nozzle
f	condition at the flame

Superscripts

$-$	in the oxygen side of the flame
$+$	in the fuel side of the flame

Also, numerical works [3–5] on multicomponent fuel droplet combustion used a single flame model to describe the burning of mixtures of heptane–hexadecane, *n*-heptane–decane and heptane–octane.

Results from asymptotical analysis showed the conditions for the burning of multicomponent fuel to proceed in a single flame. Since the reactions inside the flame can be preceded in diffusion-flame and premixed-flame regimes depending on their activation energies and the Damköhler numbers, the combination of these two burning regimes establishes the flame structure. For Damköhler numbers of the same order for all reactions, and also the activation energies, the flame presents a single diffusion-flame structure [6]. If one reaction has larger activation energy than the other reactions, two situations can be found. First, for very large Damköhler number for all reactions, the reactions proceed in diffusion-flame regime and, consequently, the flame structure is composed by two diffusion-flame structures with different thicknesses [7]. Second, if the Damköhler number of the reaction with the largest activation energy is not so large, the reaction proceeds in the premixed-flame regime, thus the flame structure is formed by the combination of a thin premixed-flame structure and a thick diffusion-flame structure; the premixed-flame structure is inside the diffusion-flame structure formed by other reactions [7]. The position of the premixed-flame structure changes with the value of the Damköhler number. The premixed-flame structure is stable inside the diffusion-flame structure meanwhile the reaction is stable with the level of oxygen found inside the diffusion-flame structure. If not, the premixed-flame structure is established out of the diffusion-flame structure and in this case the assumption of single flame is not valid.

Once the single flame assumption is held, the extended Shvab–Zel'dovich model [8–11] is able to represent multicomponent-fuel diffusion flames.

In this way, by combining the conservation equations to eliminate the chemical reaction terms, only two linear combinations are independent. The variables described by the resulting equations are the conserved scalars mixture fraction and excess enthalpy [12,9,10]. Since the oxygen and the multicomponent fuel concentrations are zero at the flame,

the mixture fraction and excess enthalpy equations are able to determine three variables, i.e. temperature, oxygen mass fraction and the mass fraction of one component of the fuel. Because the flame position is also found from the mixture fraction profile, the concentrations of the $n-1$ species are specified by the integration of their conservation equations without the chemical source term, ranging from the boundary to the flame position.

It is worth to mention that, up to now, the most general Shvab–Zel'dovich formulation, employing only the conserved scalar mixture fractions, was presented by Lam and Bellan [13] to study generically the burning of a single fuel but with complex kinetic mechanism. They included in the model the contribution of the concentration gradient on the heat transfer (Dufour effect) and temperature gradient on the mass transfer (Soret effect). Lam and Bellan combined Tambour and Gal-Or [14] procedure for decoupling the conservation equations with Dufour and Soret terms and Burke–Schumann procedure [15] for eliminating chemical reaction terms from the conservation equations to decouple the conservation equations.

In mixtures constituted by fuels with different molecular weight, the preferential mass diffusion of the light species, potentiated by the presence of heavy species, has an important influence on the flame. In addition, the preferential thermal diffusion of heavy species is augmented by the presence of light species. The importance of the mass and thermal diffusions are registered by the Lewis numbers effects.

Lewis number influence on one-fuel diffusion flames in the stable conditions (far from the extinction conditions) has been studied for a long time. The Lewis number is involved in the stoichiometric reactants fluxes conditions at the flame, thus any change of the reactants Lewis numbers represent modifications on the corresponding mass flux to the flame, forcing it to establish in different place [16]. In addition, the difference between the mass diffusion and the thermal diffusion of each reactant influentiates the flame temperature [17]. For fuels discharging in a quiescent oxidant atmosphere, the fuel Lewis number does not affect the flame temperature and affect only slightly the flame position; the oxidant Lewis number does influentiate these properties [11]. For fuel flow against oxidant flow, both Lewis numbers involve in the determination of the flame temperature and position [18]. More recently, the temporal behaviour of the diffusion flame close to the extinction condition started being studied. At this state, the diffusion flame can take a unstable cellular form [19,20].

Due to the characteristics of the problem, the influence of the Lewis number on the stable condition of the diffusion flames can be analysed. This extended Shvab–Zel'dovich formulation will be applied to *n*-heptane and hydrogen mixtures to analyse hydrocarbon diffusion flames enriched by hydrogen and hydrogen diffusion flames enriched by hydrocarbon. The choice for the fuels took into account the interest in *n*-heptane flames and hydrogen unpolluting properties, as well as, the possibility of changing the mixture Lewis number (the effective Lewis number) in a large range and studying the radiative energy loss.

2. Flowfield: model and mathematical formulation

The analysis of multicomponent fuel diffusion flames will be performed based on the counterflow configuration, which is schematically presented in Fig. 1. This configuration is broadly used in numerical and analytical analyses since the results can be verified experimentally due to the easy access into the flame. In addition, the particularities of the counterflow configuration permit several simplifications on the flow field description [21], such as

$$u/v_0 = rU(x),\ \rho v/\rho_0 v_0 = V(x),\ p/\rho_0 v_0^2 = P(x) - r^2 J/2 \tag{1}$$

where r, x, u, v, ρ, p, and J are the radial and axial coordinates nondimensionalized with the distance l between nozzles, the radial and axial component of the velocity, density, pressure, and a constant, respectively. According to Fig. 1, the oxidant stream comes out at $x=0$ and the multicomponent fuel stream comes out at $x=1$. Consequently, the subscript 0 is used to denote the condition at $x=0$ and the subscript 1 is used to denote the condition at $x=1$. The oxidant stream is constituted in a such way that Y_{O0} is the oxygen mass fraction and $(1-Y_{O0})$ is the nitrogen mass fraction. The multicomponent-fuel stream comes with mass fractions Y_{i1} for the fuels and $\left(1-\sum_{i=1}^{n} Y_{i1}\right)$ for the nitrogen mass fraction.

The n fuels chemical reactions, given in terms of mass, proceed at one global step according to the following set of reactions

$$\begin{aligned}
&F_1 + s_1 O_2 \rightarrow \tilde{c}_1 CO_2 + \tilde{h}_1 H_2O \quad (+Q_1)\\
&F_2 + s_2 O_2 \rightarrow \tilde{c}_2 CO_2 + \tilde{h}_2 H_2O \quad (+Q_2)\\
&\vdots \qquad \vdots \qquad \vdots \qquad \vdots \qquad \vdots\\
&F_n + s_n O_2 \rightarrow \tilde{c}_n CO_2 + \tilde{h}_n H_2O \quad (+Q_n),
\end{aligned}$$

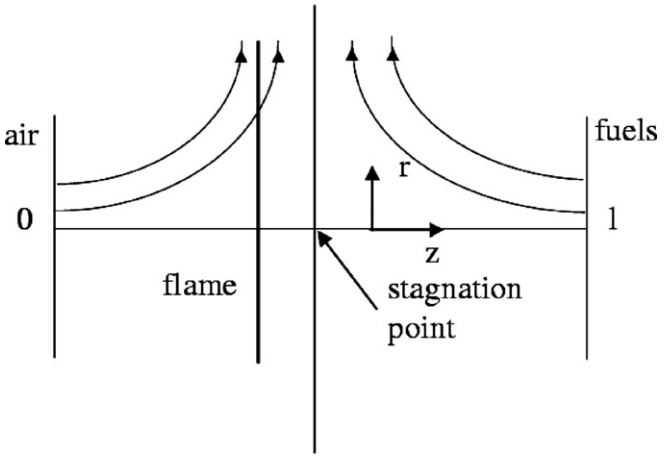

Fig. 1. Schematic representation of the counterflow geometry.

where s_i, $\tilde{c}_1$ and $\tilde{h}_i$ are the stoichiometric coefficients in terms of mass and Q_i is the heat released per unity of fuel i mass by the reaction i. The rates related with the reactions are

$$\tilde{w}_i = B_i \rho^{\beta_{i1}+\beta_{i2}} Y_O^{\beta_{i1}} Y_i^{\beta_{i2}} \mathrm{e}^{-E_i/RT}$$

where B_i, $\beta_{i\bullet}$ and E_i are the frequency factor, the global reaction order and the activation energy of reaction i, respectively.

The radiative energy transfer is included in the model by the approximation of optically thin transparent gas and released in the CO_2 and H_2O bands. The radiative energy loss is taken into account in the analysis through the term q_{rad} expressed by

$$q_{\mathrm{rad}} = \sigma\theta^4 \left(X_{\mathrm{CO_2}} \frac{\bar{l}_{\mathrm{P}}}{l_{\mathrm{P\,CO_2}}} + X_{\mathrm{H_2O}} \frac{\bar{l}_{\mathrm{P}}}{l_{\mathrm{P\,H_2O}}} \right)$$

in which θ ($\equiv T/T_0$) is the nondimensional temperature, X_i denotes the mole fraction of species i. The Planck-mean absorption lengths l_{P} for CO_2 and H_2O can be found elsewhere [22,23]. The dimensionless emissivity σ that appears in the previous equation is given by

$$\sigma = \frac{4\sigma_{\mathrm{B}} T_0^3 l}{\bar{l}_{\mathrm{P}} c_{\mathrm{p}} \rho_0 v_0}$$

where σ_{B} is the Stefan–Boltzmann constant, $\bar{l}_{\mathrm{P}}$ is the mean value between $l_{\mathrm{P\,CO_2}}$ and $l_{\mathrm{P\,H_2O}}$ evaluated at the flame position.

It was considered that the specific heat at constant pressure c_{p} is constant and that the thermal conductivity k, diffusion coefficient D, coefficient of viscosity μ depend only on temperature

$$\frac{\rho D_i}{\rho_0 D_{i0}} = \frac{k}{k_0} = \frac{\mu}{\mu_0} = \theta^{\alpha}$$

Moreover, in this model the Soret and Dufour effects were not considered.

By substituting Eq. (1) into the mass, momentum, species and energy conservation equations and applying the boundary layer approximation, the following system of equations is found

$$\frac{\mathrm{d}V}{\mathrm{d}x} + 2\rho U = 0 \tag{2}$$

$$V\frac{\mathrm{d}U}{\mathrm{d}x} - \frac{\mathrm{d}}{\mathrm{d}x}\left(\frac{Pr\theta^{\alpha}}{Pe}\frac{\mathrm{d}U}{\mathrm{d}x}\right) = J - \rho U^2 \tag{3}$$

$$Le_O V\frac{\mathrm{d}y_O}{\mathrm{d}x} - \frac{\mathrm{d}}{\mathrm{d}x}\left(\frac{\theta^{\alpha}}{Pe}\frac{\mathrm{d}y_O}{\mathrm{d}x}\right) = -\sum_{i=1}^{n} w_i \tag{4}$$

$$Le_i V\frac{\mathrm{d}y_i}{\mathrm{d}x} - \frac{\mathrm{d}}{\mathrm{d}x}\left(\frac{\theta^{\alpha}}{Pe}\frac{\mathrm{d}y_i}{\mathrm{d}x}\right) = -w_i \tag{5}$$

$$V\frac{\mathrm{d}\theta}{\mathrm{d}x} - \frac{\mathrm{d}}{\mathrm{d}x}\left(\frac{\theta^{\alpha}}{Pe}\frac{\mathrm{d}\theta}{\mathrm{d}x}\right) = \sum_{i=1}^{n} q_i w_i - q_{\mathrm{rad}} \tag{6}$$

where $y_O = Y_O/Y_{O0}$, $y_i = s_i Le_O Y_i/Y_{O0} Le_i$, recalling that s_i is the mass of oxygen necessary to react stoichiometrically with a unit mass of the fuel i, and $q_i = Q_i Y_{O0}/c_{\mathrm{p}} T_0 s_i Le_O$. Pe, Pr, and Le_i are the Peclet, Prandlt, and Lewis numbers, respectively, and are defined as

$$Pe = \frac{l v_0}{k_0/(\rho_0 c_{\mathrm{p}})}, \quad Pr = \frac{\mu_0}{k_0/c_{\mathrm{p}}}, \quad Le_i = \frac{k_0/(\rho_0 c_{\mathrm{p}})}{D_{i0}}.$$

The re-scaled mass fractions y_i ($i = 1, 2$) represents not only the mass fractions Y_i ($i = 1, 2$), but the fuel mass fraction compared to the oxygen mass fraction at $x = 1$ (Y_i/Y_{O0}), the fuel Lewis number compared to the oxygen Lewis number (Le_i/Le_0), and the stoichiometric coefficient s_i. Then, the usage of the re-scaled mass fraction y_i is more appropriated to describe combustion problem. Moreover, the derivative of y_i gives a more detailed information of the species i mass flux than the mass fraction Y_i. It is worth to note that, at the flame, the relation $-\mathrm{d}y_0/\mathrm{d}x = \sum_i^n \mathrm{d}y_i/\mathrm{d}x$ is satisfied.

The dimensionless reaction rate of fuel i is determined by

$$w_i = Da_i \varrho^{\beta_{i1}+\beta_{i2}} y_O^{\beta_{i1}} y_i^{\beta_{i2}} \mathrm{e}^{-\theta_{ai}/\theta}$$

where $\theta_{ai} = E_i/RT_0$ is the nondimensional activation energy and the Damköhler number Da_i is

$$Da_i = (B_i l/v_0)(\rho_0 Y_{O0})^{\beta_{i1}+\beta_{i2}-1} L_i^{\beta_{i2}}/(s_i Le_O)^{\beta_{i2}-1}$$

The profiles of $Y_{\mathrm{CO_2}}$ and $Y_{\mathrm{H_2O}}$ are found through the following conservation equations.

$$Le_{\mathrm{CO_2}} V\frac{\mathrm{d}y_{\mathrm{CO_2}}}{\mathrm{d}x} - \frac{\mathrm{d}}{\mathrm{d}x}\left(\frac{\theta^{\alpha}}{Pe}\frac{\mathrm{d}y_{\mathrm{CO_2}}}{\mathrm{d}x}\right) = \sum_{i=1}^{n} c_i w_i \tag{7}$$

$$Le_{\mathrm{H_2O}} V\frac{\mathrm{d}y_{\mathrm{H_2O}}}{\mathrm{d}x} - \frac{\mathrm{d}}{\mathrm{d}x}\left(\frac{\theta^{\alpha}}{Pe}\frac{\mathrm{d}y_{\mathrm{H_2O}}}{\mathrm{d}x}\right) = \sum_{i=1}^{n} h_i w_i \tag{8}$$

where $c_i = Y_{O0} Le_{\mathrm{CO_2}} \tilde{c}_i/Le_O s_i$ and $h_i = Y_{O0} Le_{\mathrm{H_2O}} \tilde{h}_i/Le_O s_i$. It was assumed $y_{\mathrm{CO_2}} = Y_{\mathrm{CO_2}}$ and $y_{\mathrm{H_2O}} = Y_{\mathrm{H_2O}}$ in order to follow the nomenclature used in the above equations.

The boundary conditions for the set of equations (2)–(8), are given by

$$U = V - 1 = \theta - 1 = y_O - 1 = y_i = y_{\mathrm{CO_2}} = y_{\mathrm{H_2O}} = 0 \quad \text{at } x = 0, \tag{9}$$

$$U = V - V_1 = \theta - \theta_1 = y_O = y_i - y_{i1} = y_{\mathrm{CO_2}} = y_{\mathrm{H_2O}} = 0 \quad \text{at } x = 1. \tag{10}$$

The momentum imposed on the streams at the nozzle exits specify the location of the stagnation point x_s, which is determined by the condition $V = 0$ and $\mathrm{d}U/\mathrm{d}x = 0$. The position of the flame x_{f}, characterised by the condition $y_i = y_O = 0$, is imposed by the hydrodynamic problem, the fuels and oxidant Lewis numbers, and fuels and oxidant concentrations in the streams.

The flow field of the counterflow configuration can be divided into two regions according to the flow regime. In the region close to the nozzles, the flow is in the inviscid regime. In the region near the plan that is perpendicular to the symmetric axis and has the stagnation point, the flow is characterised by the viscous regime. The thickness of the viscous layer is of the order of $(Pe^{-1})^{1/2}$ about that plan. In addition, diffusion flames estabilize inside the viscous layer

and their positions depend on the oxygen and multicomponent fuel concentrations and their Lewis numbers.

3. Burke–Schumann limit

Diffusion flame description imposing the Burke–Schumann kinetic model is relatively simple because there is no leakage of fuels and oxidant through the flame, $y_0.y_i = 0$. Consequently, the flow field can be specified by the reactants properties and the boundary conditions without any information of the chemical reaction. Despite the simplicity of the mechanism, results obtained are good to describe the problem with small leakage.

From the flow field analysis, fuels and oxidant fluxes to and the heat fluxes from the flame are determined. By knowing these properties, the consumption of the fuels and the heat released are estimated.

The system of nondimensional conservation equations for species and energy that describes multicomponent fuel diffusion flames in the Burke–Schumann limit is written in the following form

$$V\frac{\mathrm{d}}{\mathrm{d}x}\begin{vmatrix} Le_1 & 0 & \cdots & 0 & 0 & 0 \\ 0 & Le_2 & \cdots & 0 & 0 & 0 \\ \vdots & \vdots & \cdots & \vdots & \vdots & \vdots \\ 0 & 0 & \cdots & Le_n & 0 & 0 \\ 0 & 0 & \cdots & 0 & Le_O & 0 \\ 0 & 0 & \cdots & 0 & 0 & 1 \end{vmatrix}\begin{vmatrix} y_1 \\ y_2 \\ \vdots \\ y_n \\ y_O \\ \theta \end{vmatrix} - \frac{\mathrm{d}}{\mathrm{d}x}\left(\begin{vmatrix} & & & & & \\ & & & & & \\ & & & & & \\ & & & & & \\ \frac{\theta^\alpha}{Pe}\frac{\mathrm{d}}{\mathrm{d}x} & & & & & \\ & & & & & \end{vmatrix}\begin{vmatrix} y_1 \\ y_2 \\ \vdots \\ y_n \\ y_O \\ \theta \end{vmatrix}\right)$$

$$= \begin{vmatrix} -1 & 0 & \cdots & 0 \\ 0 & -1 & \cdots & 0 \\ \vdots & \vdots & \cdots & \vdots \\ 0 & 0 & \cdots & -1 \\ -1 & -1 & \cdots & -1 \\ q_1 & q_2 & \cdots & q_n \end{vmatrix}\begin{vmatrix} w_1 \\ w_2 \\ \vdots \\ w_n \end{vmatrix} - \begin{vmatrix} 0 \\ 0 \\ \vdots \\ 0 \\ 0 \\ q_{\mathrm{rad}} \end{vmatrix}. \tag{11}$$

By combining Eq. (11) according to the Shvab–Zel'dovich procedure, the reaction terms can be eliminated. The $(n+2)\times n$ matrix, which multiplies the reaction terms, has a rank $n \times n$ and the rows make a vectorial base. Moreover, the last two rows can be expressed in terms of that vectorial base. In addition, independently of the number of species in the fuel, there are only two combinations among the equations that lead to equations without chemical source term. The two conserved functions that satisfy those equations are the mixture fraction and the excess enthalpy [12,8,9] given by

$$Z = \sum_{i=1}^{n} y_i - y_O + 1 \tag{12}$$

$$H = \sum_{i=1}^{n} (q_i - 1)y_i + y_O + \theta \tag{13}$$

which are obtained by multiplying the system of Eq. (11) by the following matrix

$$\begin{vmatrix} 1 & 1 & \cdots & 1 & -1 & 0 \\ q_1 - 1 & q_2 - 1 & \cdots & q_n - 1 & 1 & 1 \end{vmatrix}$$

From Eq. (13) and the condition of $y_0 = y_i = 0$ at the flame, the flame position in terms of the mixture fraction Z is at $Z = 1$.

In problems with infinite chemical reaction rate, the excess enthalpy leads to flame temperature different from the adiabatic value. For fuel Lewis number smaller than unity, the flame temperature is higher than the adiabatic flame temperature and for that higher than unity the flame temperature is smaller than the adiabatic flame temperature. Only for Lewis number equal to one, the flame temperature is equal to the adiabatic flame temperature.

The conservation equations for the functions Z and H are given by the following equations [11]:

$$V\frac{\mathrm{d}}{\mathrm{d}x}\left(\int_0^Z L(Z)\mathrm{d}Z\right) - \frac{\mathrm{d}}{\mathrm{d}x}\left(\frac{\theta^\alpha}{Pe}\frac{\mathrm{d}Z}{\mathrm{d}x}\right) = S_Z \tag{14}$$

$$V\frac{\mathrm{d}}{\mathrm{d}x}\left(H + \int_0^Z N(Z)\mathrm{d}Z\right) - \frac{\mathrm{d}}{\mathrm{d}x}\left(\frac{\theta^\alpha}{Pe}\frac{\mathrm{d}H}{\mathrm{d}x}\right) = S_H - q_{\mathrm{rad}} \tag{15}$$

The distributed source terms, S_Z and S_H, which appear in the foregoing equations are defined as,

$$S_Z = \begin{cases} 0 & Z < 1 \\ V\sum_{i=2}^{n}(Le_1 - Le_i)\mathrm{d}y_i/\mathrm{d}x & Z > 1 \end{cases}$$

$$S_H = \begin{cases} 0 & Z < 1 \\ V\sum_{i=2}^{n}[(Le_1 - 1)(q_1 - 1) - (Le_i - 1)(q_i - 1)]\mathrm{d}y_i/\mathrm{d}x & Z > 1 \end{cases}$$

and the function $L(Z)$ and $N(Z)$ are

$$L(Z) = \begin{cases} Le_O, & Z < 1 \\ Le_1, & Z > 1 \end{cases},$$

$$N(Z) = \begin{cases} (1 - Le_O), & Z < 1 \\ (Le_1 - 1)(q_1 - 1), & Z > 1 \end{cases},$$

As can be seen from Eqs. (14) and (15), the difference in the speed of the massic and thermal transports is the source for mixture fraction Z and the excess enthalpy H. Also, the determination of $n+1$ variables in the fuels side of the flame $y_1, y_2, \ldots, y_n$ and θ is not possible from Eqs. (14) and (15). Nevertheless, as the flame is found by the condition $Z = 1$, the conservation equations of $n-1$ species can be written as,

$$Le_i V\frac{\mathrm{d}y_i}{\mathrm{d}x} - \frac{\mathrm{d}}{\mathrm{d}x}\left(\frac{\theta^\alpha}{Pe}\frac{\mathrm{d}y_i}{\mathrm{d}x}\right) = 0, \quad \text{for } i = 2, \ldots, n \tag{16}$$

which, at the flame, must satisfy the condition

$$y_i = 0, \text{ at } Z(x = x_{\mathrm{f}}) = 1. \tag{17}$$

Besides the necessity of integrating Eqs. (16), the extended Shvab–Zel'dovich formulation for multicomponent fuel diffusion flames differs from that one for one-fuel diffusion flame by the source terms S_Z and S_H. These source terms take into account for the differences of diffusivity among the species, in the same way of that term represented by

the integration of function $N(Z)$. Therefore, if the Lewis numbers are unity, the source terms become zero, $L-1=N=S_Z=S_H=0$, and the problem is simpler to be solved.

In the Burke–Schumann limit, the reaction terms in the balance equations can be substituted by the Dirac function, $w_i=\bar{w}_i\delta(x-x_f)$. Thereby, the rate of each reaction $\bar{w}_i$ is determined by the integration of the corresponding balance equation around the flame

$$\left.\frac{\theta_f^\alpha}{Pe}\frac{dy_i}{dx}\right|_{x=x_f^+}=\bar{w}_i \tag{18}$$

From Eq. (18), the conservation equations for CO_2 and H_2O are given by,

$$Le_{CO_2}V\frac{dy_{CO_2}}{dx}-\frac{d}{dx}\left(\frac{\theta^\alpha}{Pe}\frac{dy_{CO_2}}{dx}\right)=\left(\frac{\theta_f^\alpha}{Pe}\sum_{i=1}^{n}c_i\left.\frac{dy_i}{dx}\right|_{x=x_f^+}\right)\delta(x-x_f) \tag{19}$$

$$Le_{H_2O}V\frac{dy_{H_2O}}{dx}-\frac{d}{dx}\left(\frac{\theta^\alpha}{Pe}\frac{dy_{H_2O}}{dx}\right)=\left(\frac{\theta_f^\alpha}{Pe}\sum_{i=1}^{n}h_i\left.\frac{dy_i}{dx}\right|_{x=x_f^+}\right)\delta(x-x_f) \tag{20}$$

Therefore, multicomponent fuel counterflow diffusion flames are described by Eqs. (2), (3), (14)–(17), (19) and (20) with the following boundary conditions,

$$V-1=U=\theta-1=y_i=y_O-1=y_{H_2O}=y_{CO_2}=H-2=Z=0 \quad \text{at } x=0 \tag{21}$$

$$V-V_1=U=\theta-\theta_1=y_i-y_i=y_O=y_{H_2O}=y_{CO_2}=H-H_1=Z-Z_1=0 \quad \text{at } x=1 \tag{22}$$

where

$$V_1=\rho_1v_1/\rho_0v_0,\ \theta_1=T_1/T_0,$$

$$H_1=\sum_{i=1}^{n}[(q_i-1)y_{i1}+\theta_1] \text{ and } Z_1=\sum_{i=1}^{n}y_{i1}+1$$

By considering the Burke–Schumann limit, discontinuity is imposed on all derivatives of the dependent variables at the flame, $x=x_f$. However, as can be seen in Eqs. (14) and (15), the Shvab–Zel'dovich formulation relaxes this condition only on the first derivative, i.e., Z and H functions and their first derivatives are continuous [24]. The continuity condition does not reach higher order derivatives because S_Z and S_H are discontinuous at the flame. It is worthwhile to note that the discontinuity on $L(Z)$ and $N(Z)$ functions were removed by considering their integrals.

For the particular case of equal Lewis numbers, $Le_1=Le_2=\cdots=Le_n=Le$, the discontinuity that appears on S_Z is removed. Moreover, the integration of Eq. (16) becomes unnecessary and the profiles for y_i are found by $y_i=y_{i1}(Z-1)/(Z_1-1)$. Also, the source term S_H simplifies to the following equation for $Z>1$:

$$S_H=V(Le-1)\sum_{i=2}^{n}(q_1-q_i)\frac{dy_i}{dx}.$$

For the special case of Lewis numbers unity for fuels and oxygen, the source term originated by the difference between mass and heat transports vanishes. Moreover, if the radiative energy losses could be neglected, then the H and Z functions would become similar, as seen in Eqs. (14) and (15), $Z/Z_1=(H-2)/(H_1-2)$ [25].

4. Results and comment

An extended Shvab–Zel'dovich formulation is applied to n-heptane-hydrogen counterflow diffusion flames. Despite the choice of working with a minimum number of species to characterise multicomponent fuel, it represents a multicomponent fuels composed by heavy fuels with small diffusion velocity and large conduction velocity (Lewis number larger than unity), and light fuels with large diffusion velocity and small conduction velocity (Lewis number lower than unity).

The characteristic of the counterflow problem is given by the following properties. The space between the two nozzles is set to $l=2$ cm, the fuel mass fluxes and the temperature, fixed at 373 K for all cases, are the same for the two streams at the nozzles; $V_0=-V_1=1$ and $\theta_0=\theta_1=1$. The Lewis numbers $(k_0/c_p\rho_0)/D_{i0}$, are different from unity ($k_0=0.0303$ J/m K s). The n-heptane, hydrogen, oxygen, water vapour and carbon dioxide Lewis numbers are 1.7, 0.5, 1.1, 0.85 and 1.2, respectively.

Here the n-heptane is labelled by species 1 and hydrogen is labelled by species 2. Then, chemical reaction parameters are defined by $s_1=3.52$, $\tilde{h}_1=3.08$, $\tilde{c}_1=1.44$ for the single global step reaction of n-heptane and oxygen and by $s_2=8$, $\tilde{h}_2=9$, $\tilde{c}_2=0$ for the single global step reaction of hydrogen and oxygen. The heat released by the n-heptane reaction is 4.495×10^4 (J/kg) and by the hydrogen reaction is 1.198×10^5 (J/kg).

The results presented in this section are obtained by the numerical integration of the multicomponent-fuel diffusion flame problem, described by Eqs. (2), (3), (14)–(17), (19) and (20) satisfying the boundary conditions, Eqs. (21) and (22). The numerical scheme is based on the finite difference. The first derivatives are represented by a backward difference in the part of the domain in which V is positive, but by a forward difference in the other part of the domain in which V is negative. The condition $V>0$ is found between the oxidant nozzle and the stagnation point, and the condition $V<0$ is found between the stagnation point and the fuel nozzle.

The position of the flame x_f is determined in terms of the distance between the two nozzles. Sometimes, it is more significant to specify the position of the flame inside the viscous layer. For that, it will be used the Liñán's parameter γ [26], defined as $\gamma=(d_\theta^+-d_\theta^-)/(d_\theta^++d_\theta^-)=1-2d_\theta^-/(d_\theta^++d_\theta^-)$, in which $d_\theta^-=d\theta/dx|_{x=x_f^-}$ and $d_\theta^+=-d\theta/dx|_{x=x_f^+}$. The γ measures the normalised heat flux from the flame to the fuel stream relatively to that to the air stream. Consequently, $\gamma>0$ means that the heat flux to the fuel side of the flame is larger than that to the air side of the flame

and $\gamma < 0$ means that the heat flux to the air side is larger. Furthermore, for $\gamma > 0$ the flame is in the part of the viscous layer facing the fuel nozzle and for $\gamma < 0$ the flame is in the part of the viscous layer facing the oxidant nozzle.

There are three particular cases $\gamma = -1, 0, 1$. For $\gamma = 0$, the heat released by the reactions is equally transferred to both sides of the flame, the flame occupied the central part of the viscous layer, on the plane having the stagnation point. For $\gamma = -1$, the heat released by the reactions is integrally transferred to the oxygen side of the flame and for this to happen the flame has to occupy the oxygen border of the viscous layer. For $\gamma = 1$, the heat is transferred to the fuel side and the flame has to take place at the fuel border of the viscous layer.

The results will be presented in three sections.

The first part displays the rules of the preferential mass diffusion of hydrogen and thermal diffusion of *n*-heptane, through the Lewis numbers of the fuels, on the properties of the multicomponent fuel diffusion flame.

The second part of this section exhibits the flow stretch influence (by the reciprocal scalar dissipation χ_f^{-1}) on the flame. In this part, the effect of the radiative energy loss is revealed. For that, a fix composition for the mixture is adopted and the oxidant and fuels streams velocities are changed. The stretch influence is exhibited in terms of the reciprocal scalar dissipation χ_f^{-1} to conform the presentation to flamelet theory [27]. The reciprocal of the scalar dissipation χ_f^{-1} is defined as $\{2(k/\rho c_p)(1/l^2)[\vec{\nabla}(Z/Z_1)]^2|_{x=x_f}\}^{-1} = \{2(k_0/\rho_0 c_p)(1/l^2)\theta_f^{1+\alpha}[\vec{\nabla}(Z/Z_1)]^2|_{x=x_f}\}^{-1}$, whose unit is s.

The third part shows the influence of hydrogen doping on *n*-heptane diffusion flames and the *n*-heptane doping in hydrogen diffusion flames. To evaluate the effects of the doping on the flames, a fixed and small quantities in terms of mass of hydrogen is mixed with *n*-heptane and nitrogen in the fuels stream.

The presentation of the results for γ and χ_f^{-1} seems senseless because they are not characteristic parameters of the model established in this work. However, their exhibition will help future analyses concerning to multicomponent-fuels diffusion flame extinction problems.

5. Lewis number effects

To highlight the Lewis number effects on the flame, the loss of energy by thermal radiation is excluded from the model and the total heat release is fixed for any mixture of *n*-heptane and hydrogen. Even with these two considerations, the influence of the preferential mass diffusion is not isolated completely from the other effects. The variation of the total specific heat with the composition cannot be avoided. A way to expose only the Lewis number effects on the flame is to present the results relative to the adiabatic case (unity Lewis number), in which only the total specific heat is varying with composition.

First of all, the absolute results with the effects of the nonunity Lewis number are depicted. In the following, the relative results to the unity Lewis number are shown.

The value for the fixed total heat release could be any one in the range between the *n*-heptane and hydrogen heat release. The adopted value is equal to the *n*-heptane heat release, thereby the mass fractions of *n*-heptane and hydrogen follow the expression $Y_{11} = 1 - (Q_2/Q_1)Y_{21} = 1 - 2.665\,Y_{21}$; seen in Fig. 2a. The maximum hydrogen mass fraction is found $Y_{21} = 0.375$, for $Y_{11} = 0$.

Fig. 2b presents the effective Lewis number, whose rule to specify it is $Le_{ef} = \sum_i^n Y_{i1} Le_i / \sum_i^n Y_{i1}$, as a function of the hydrogen mass fraction Y_{21}. The data correspond to four sets of Lewis numbers (Le_1, Le_2); (1.0, 1.0), (1.7, 1.0), (1.0, 0.5), and (1.7, 0.5). The first three sets are imposed in the model with the aim to highlight the influence of the effective Lewis numbers on the flame properties. According to the mixing rule adopted to specify the effective Lewis number and to the rule to determine the mixtures, the fourth set of Lewis numbers (1.7, 0.5) leads to effective Lewis numbers larger than unity in the most part of the range for Y_{21}, $0 \leqslant Y_{21} < 0.3$.

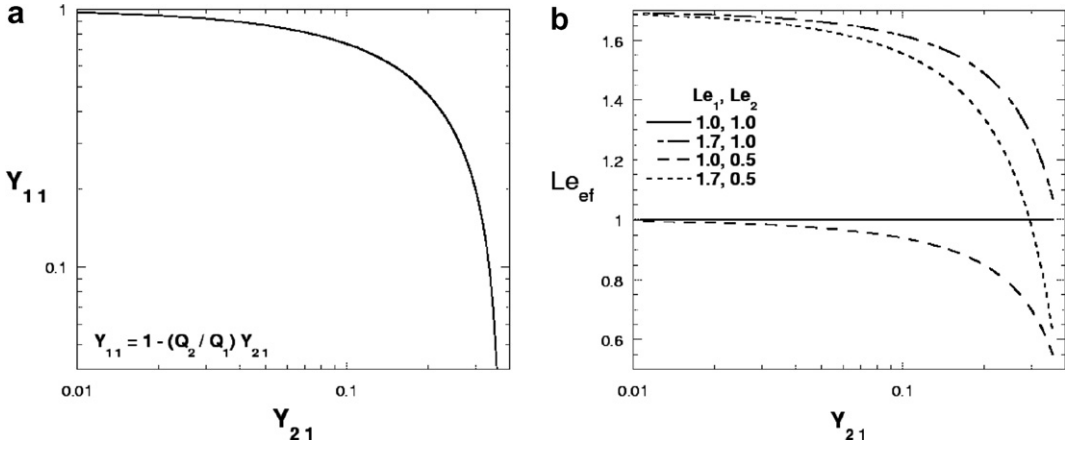

Fig. 2. (a) The mass fractions of the *n*-heptane and hydrogen mixtures considered. (b) Effective Lewis number $Le_{ef} = \sum_i^n Y_{i1} Le_i / \sum_i^n Y_{i1}$.

As knowing, the temperature for one-fuel diffusion flame depends on the Lewis numbers of the reactants. Fuels with lower Lewis numbers establish flames with higher temperatures. For Lewis numbers lower than unity, the flame temperature is larger than that for the adiabatic condition (unity Lewis number). For multicomponent-fuels diffusion flames, the same dependence to the flame temperature on the effective Lewis number is found for some mixture compositions ($Y_{21} < 0.1$) in the cases $(1.0, 0.5)$ and $(1.7, 0.5)$ and for other mixture compositions ($Y_{21} < 0.2$) in the cases $(1.0, 1.0)$ and $(1.7, 1.0)$, as seen in Fig. 3a. Note that the flame temperature θ_f, corresponding to unity effective Lewis number $Le_{ef} = 1$, changes with the composition because the fuels mixture specific heat at constant pressure changes with the composition.

However, the flame temperature behaviour with the effective Lewis number changes for other mixture compositions ($Y_{21} > 0.1$), as seen in the cases $(1.7, 0.5)$ and $(1.0, 0.5)$. The flame temperature in the case $(1.7, 0.5)$ is larger than that in the case $(1.0, 0.5)$, which the effective Lewis number in the first case is larger than that in the second case, as seen in Figs. 3a and 2b, respectively. The same features occur between the cases $(1.7, 1.0)$ and $(1.0, 1.0)$ in the range $Y_{21} > 0.2$. This behaviour is explained by the fact that the presence of the *n*-heptane molecule in mixtures of nitrogen and hydrogen potentiates the hydrogen mass diffusion. At the same time, the presence of hydrogen in mixtures of nitrogen and *n*-heptane also potentiates the *n*-heptane thermal diffusion.

Therefore, by increasing the hydrogen mass fraction in mixtures, in which the majority species are nitrogen and *n*-heptane, the flame temperature increases due to the preferential hydrogen mass diffusion, as can be seen in the cases $(1.7, 1.0)$, $(1.0, 0.5)$ and $(1.7, 0.5)$. However, in these three cases, the flame temperature presents a maximum value that corresponds to the balance between the preferential hydrogen mass diffusion and *n*-heptane thermal diffusion. For mixtures with larger hydrogen mass fraction, the *n*-heptane becomes a minority species in the mixture and the preferential *n*-heptane thermal diffusion is responsible for reducing the flame temperature, as seen in Fig. 3a.

An analysis of the source terms S_Z and S_H, Eqs. (14) and (15), reveals the behaviour of the mixture fraction Z and excess enthalpy H, consequently, of the flame temperature θ_f, as a function of the preferential hydrogen mass diffusion and *n*-heptane thermal diffusion. Since the flame occupies a position in the flowfield where $V > 0$ (as pointed by $\gamma < 0$) and $dy_2/dx|_{x=x_f} > 0$, the source term S_Z $(Z \geqslant 1) = (Le_1 - Le_2)V\ dy_2/dx$ becomes larger as larger the difference $(Le_1 - Le_2)$ is. In the same way, the source

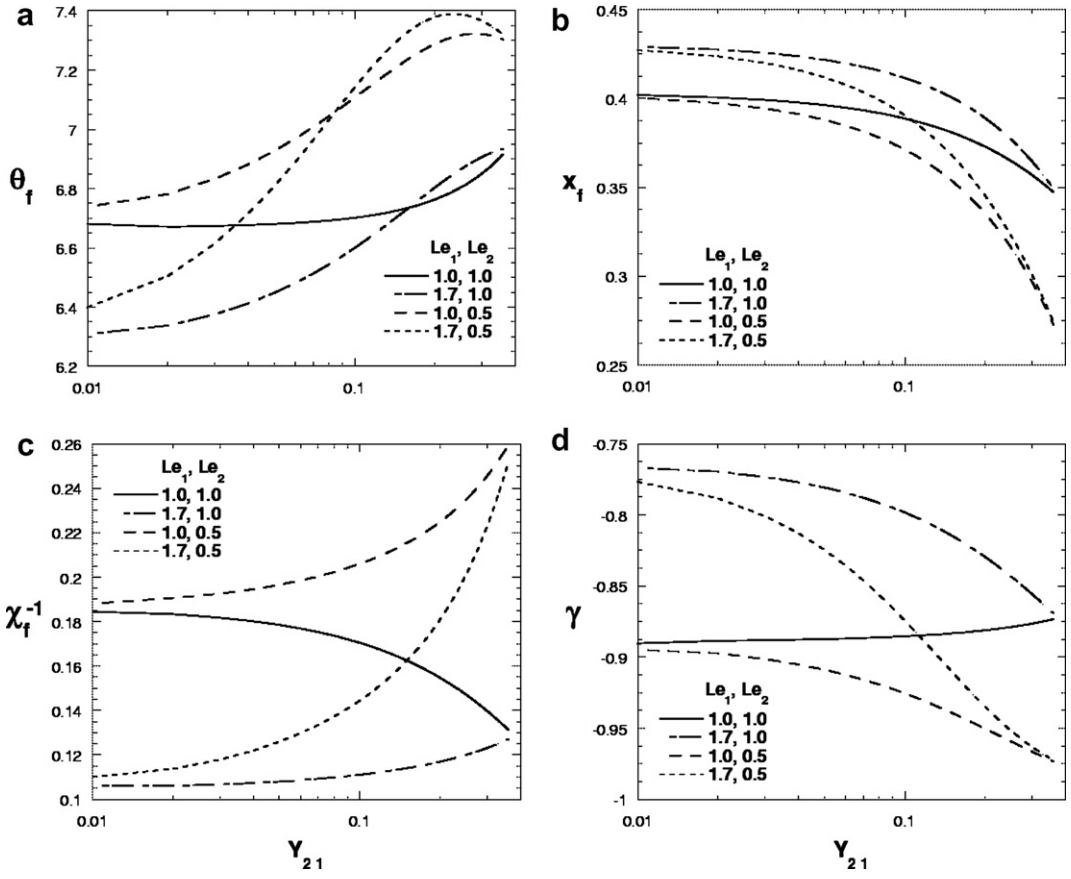

Fig. 3. (a) Flame temperature θ_f; (b) flame position x_f; (c) reciprocal scalar dissipation χ_f^{-1} and (d) the Liñán's parameter γ as a function of the hydrogen mass fraction Y_{21}.

term $S_H(Z \geqslant 1) = [(Le_1 - 1)(q_1 - 1) - (Le_2 - 1)(q_i - 1)]V$ dy_2/dx increases as larger Le_1 is and as smaller Le_2 is. Consequently, an increase in the excess enthalpy H due to an increase in the source term S_H leads to an increase in the flame temperature. Therefore, even though the potentiated transport processes produced by presence of heavy and light species in ternary mixtures with nitrogen were not taken into account, the extended Shvab–Zel'dovich formulation is able to describe those processes gathering the influence of each species in the terms $(Le_1 - Le_2)$ and $[(Le_1 - 1)(q_1 - 1) - (Le_2 - 1)(q_i - 1)]$.

The behaviour of the flame position x_f as a function of the effective Lewis number for multicomponent-fuel burning is the same to that for single-fuel burning. Then, as lower the effective Lewis number is, as closer the flame is established to the oxidant nozzle to satisfy the stoichiometric conditions for the reactants mass fluxes, as shown in Fig. 3b.

The influence of the effective Lewis number on the reciprocal scalar dissipation χ_f^{-1} is depicted in Fig. 3c. The results present low values for χ_f^{-1} with large values for Le_{ef}. This is so because an increase in Le_{ef} causes an increase in ∇Z, imposing a reduction in χ_f^{-1}. It is also observed an increase in the χ_f^{-1} in terms of Y_{21}, explained by the increase of $Z_1 = \sum_i^n y_{i1} + 1 = \sum_i^n s_i Le_O Y_{i1}/Y_{O0} Le_i + 1$. The results corresponding to (1.0, 1.0) has, for any mixture composition, a constant effective Lewis number, thus a change in the composition does not modify significantly the term $\nabla Z/Z_1$. However, an increase in Y_{21} causes a reduction on the specific heat c_p and, consequently, on the reciprocal scalar dissipation χ_f^{-1}.

Fig. 3d shows the dependence of the heat fluxes, by the Liñán's parameter γ, on the composition of the fuels mixtures. Due to the geometry of the flow field, the heat fluxes from the flame depends on the flame position inside the viscous layer. As seeing in Fig. 2b, increasing the presence of the hydrogen in the mixture, the value of the effective Lewis number decreases and, thereby, the flame establishes closer to the oxygen nozzle in order to satisfy the stoichiometric condition for the reactants fluxes, Fig. 3b. Thereby, increasing Y_{21}, the heat flux to the oxygen side of the flame increases, this reflects on the parameter γ which becomes closer to the value -1.

The effects of the fuels Lewis numbers are exhibited in Fig. 4. As mentioned before, to evidentiate only the dependence of the flame properties on the Lewis numbers, the results are presented relatively to the adiabatic case ($Le_1 = 1$, $Le_2 = 1$). No further comments on the results depicted in this figure are necessary because they confirm previous results.

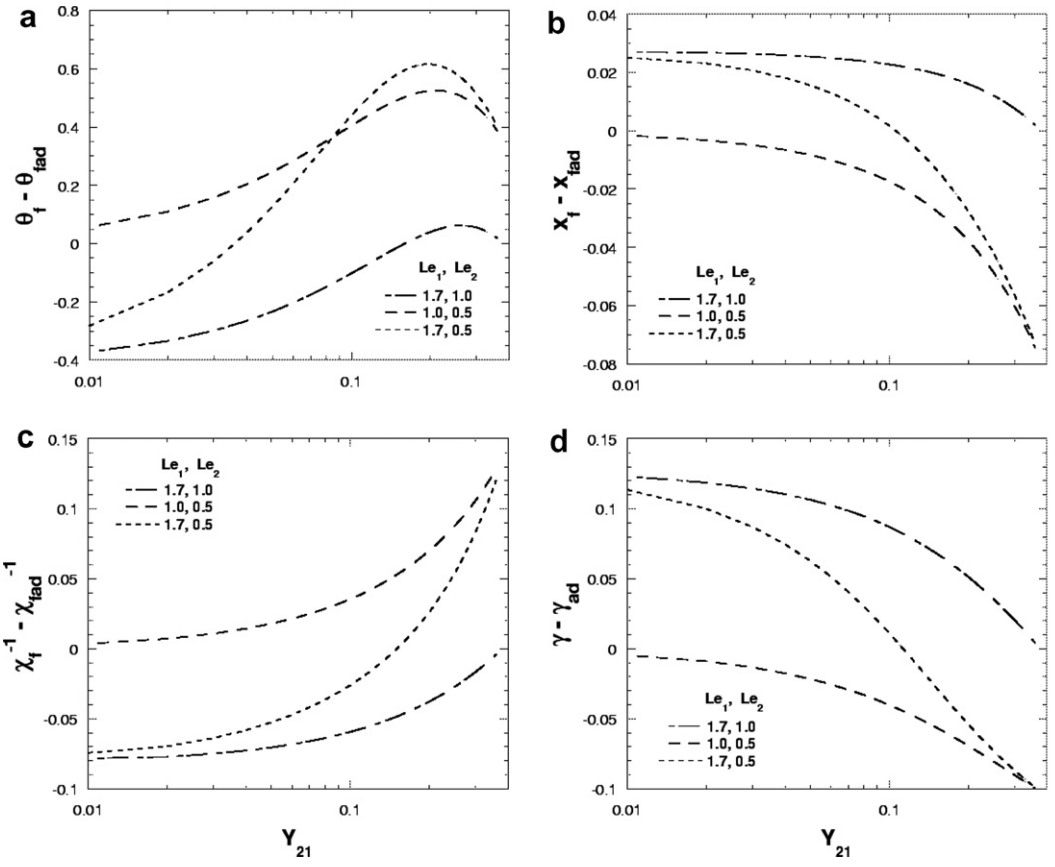

Fig. 4. (a) Relative flame temperature $\theta_f - \theta_{fad}$; (b) relative flame position $x_f - x_{fad}$; (c) relative reciprocal scalar dissipation $\chi_f^{-1} - \chi_{fad}^{-1}$ and (d) relative Liñán's parameter $\gamma - \gamma_{fad}$ as a function of the hydrogen mass fraction Y_{21}.

6. Scalar dissipation effects

In the formulation, besides the oxidant and fuel Lewis numbers, the characteristic parameter is the Peclet number or its reciprocal. It would be expected the result presentation in terms of the Peclet number or its reciprocal, however, the results will be exposed in terms of the reciprocal scalar dissipation χ_f^{-1} to adequate to the flamelet theory.

It is worth to recall that the radiative energy loss is included in the model hereafter.

Fig. 5 presents the reciprocal Peclet number Pe^{-1} as a function of the reciprocal scalar dissipation χ_f^{-1}, for three fuel compositions. According to this plot, there is a relationship between Pe^{-1} and χ_f^{-1} given by $Pe^{-1} = C(\chi_f^{-1})^a$, which the exponent a is around one and the constant of proportionality C depends on fuels mixture. The results indicate that, by increasing the hydrogen mass fraction Y_{21}, but keeping the total fuel mass fraction constant ($Y_{11} + Y_{21} = 0.4$), the flame temperature θ_f, the mixture fraction Z_1 and the gradient of Z increase too. However, the increase of $\theta_f^{1+\alpha}|\widetilde{\nabla Z}|^2$ is not large enough to compensate the increase of Z_1^2, thereby χ_f^{-1} increases with an increase of the hydrogen mass fraction in the mixture.

The quantitative behaviour of the flame temperature θ_f as a function of the reciprocal scalar dissipation χ_f^{-1} is observed in Fig. 6a. The presence of hydrogen in the mixture leads to higher flame temperature. The increase in the flame temperature is produced by three factors. First, since the heat released by the hydrogen reaction is larger than

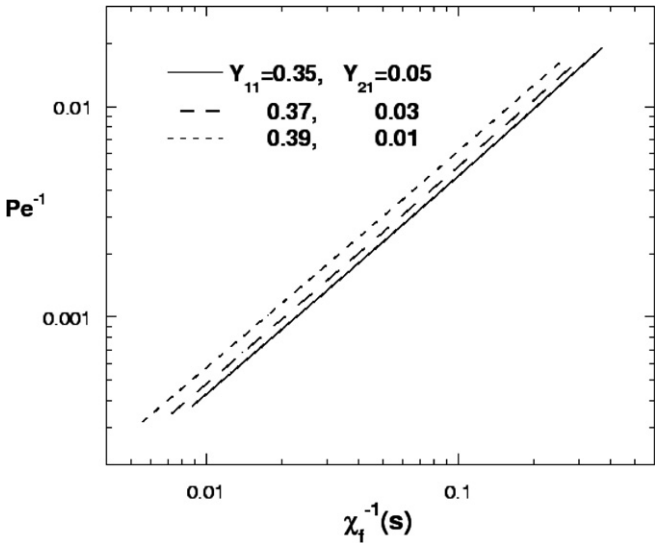

Fig. 5. The reciprocal scalar dissipation χ_f^{-1} as a function of the reciprocal Peclet number Pe^{-1} for four fuel compositions.

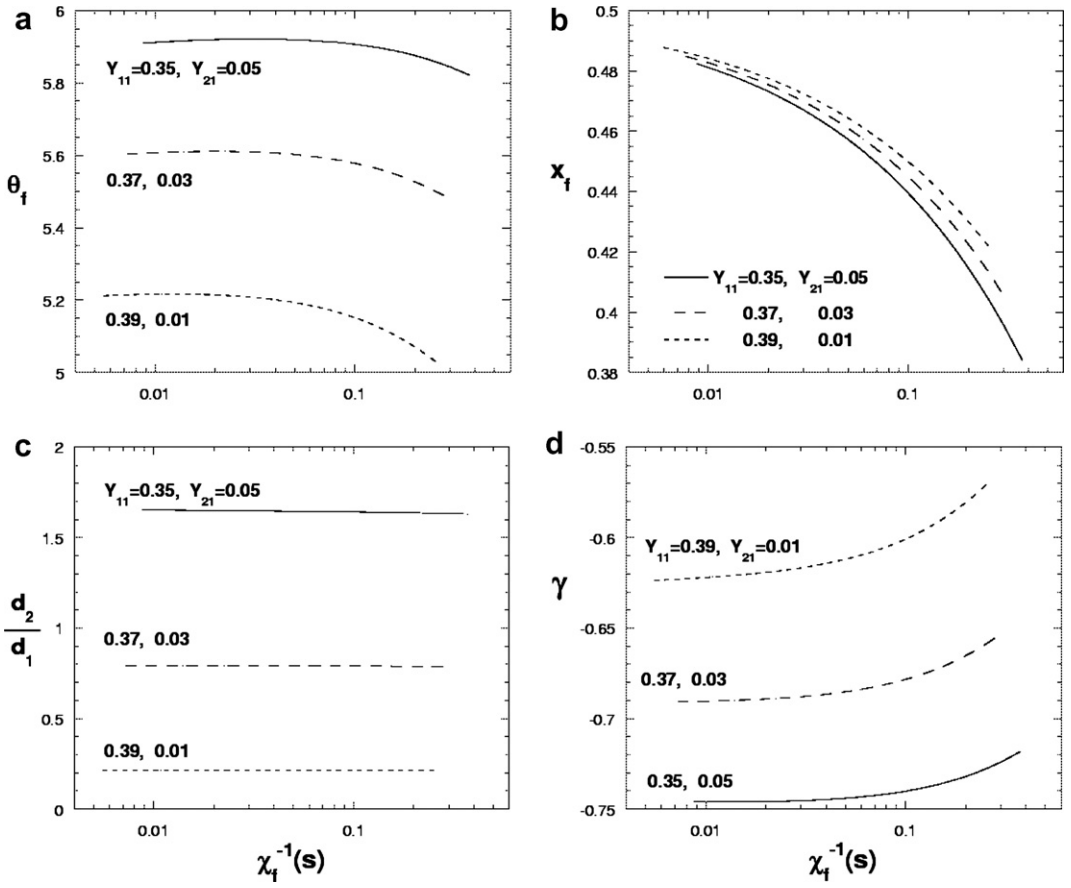

Fig. 6. Distribution of (a) flame temperature θ_f; (b) flame position x_f; (c) ratio d_2/d_1 and (d) the Liñán's parameter γ as a function of the reciprocal scalar dissipation χ_f^{-1}; for three composition (Y_{11}, Y_{21}): (0.35, 0.05), (0.37, 0.03) and (0.39, 0.01).

the *n*-heptane reaction, the total heat released increases with an increase of the hydrogen concentration. Second, because the hydrogen Lewis number is smaller than that of the *n*-heptane, the effective Lewis number decreases with the hydrogen mass fraction in the mixture, and consequently, the flame temperature is augmented. Third, the CO_2 concentration reduces with an increase of the hydrogen concentration and this leads to a decrease in the radiative heat loss.

Another feature observed from Fig. 6a is the variation in the flame temperature θ_f caused by the change of the reciprocal scalar dissipation χ_f^{-1}. By increasing χ_f^{-1}, the viscous layer becomes wider as well as the hot gases zone, from which the thermal radiation is generated. Thereby, the radiative energy loss becomes large by increasing χ_f^{-1}, consequently, the flame temperature reduces.

Fig. 6b shows the flame position x_f as a function of χ_f^{-1}. As knowing, the flame position is determined by the condition of stoichiometry of the reactants mass fluxes. Because the stoichiometric coefficients s_i/Y_{O0} is large, the flame estabilizes close to the border of the viscous layer in the oxygen side. Therefore, increasing χ_f^{-1}, the viscous layer becomes wider and consequently the flame is closer to the oxygen stream nozzle. This is confirmed by Fig. 6b.

Let d_1 and d_2 be the *n*-heptane and hydrogen mass fluxes to the flame, respectively. Thus $d_1 = \mathrm{d}y_1/\mathrm{d}x|_{x=x_f^+}$ and $d_2 = \mathrm{d}y_2/\mathrm{d}x|_{x=x_f^+}$. As will be seen, although the presence of the hydrogen in the mixture is very small, $Y_{21} \leqslant 0.05$, the hydrogen mass flux d_2, in terms of the modified mass fraction y_i, to the flame is comparable to the *n*-heptane mass flux. The ratio d_2/d_1 will show the importance of the hydrogen, even for small concentrations (in terms of mass) in hydrocarbon diffusion flames.

According to Fig. 6c, only a very small variation is observed on the ratio d_2/d_1 in the investigated range for χ_f^{-1}. Thereby, this behaviour justifies the assumption of d_2/d_1 to be practically independent of the scalar dissipation and dependent only on the composition of the fuels mixture. Fig. 6d displays the value of the γ as a function of χ_f^{-1}. All results satisfy $\gamma < 0$, then the flame is in the oxygen side of the viscous layer. Increasing the presence of the hydrogen in the mixture, $-\gamma$ increases. This result indicates that the flame establishes closer to the viscous layer border in the oxygen side as higher hydrogen concentration is.

7. Doping effect

In this section, hydrogen doping on the *n*-heptane diffusion flames as well as *n*-heptane doping on hydrogen diffusion flames are analysed. The *n*-heptane doping is qualitatively observed for mixtures with Y_{11} close to 0.1.

The dependences of the reciprocal scalar dissipation χ_f^{-1}, the reciprocal Peclet number Pe^{-1}, flame temperature θ_f, the ratio d_1/d_2 and the parameter γ on the mixture composition are illustrated in Fig. 7a to Fig. 7d. In these figures, the results are displayed for fix quantities of hydrogen $Y_{21} = 0.05$, 0.03, 0.01 and *n*-heptane varying from $Y_{11} = 0.95$, 0.97, 0.99, respectively, to $Y_{11} = 0.10$. The plots correspond to a gas velocity at the oxidant nozzle of 2m/s.

Fig. 7a shows the variation of the reciprocal scalar dissipation χ_f^{-1} and the reciprocal Peclet number Pe^{-1} as a function of the *n*-heptane mass fraction Y_{11}. The large variation of the reciprocal of scalar dissipation χ_f^{-1} confirms its main dependence on the composition of the fuel mixture. The small variation of the Pe^{-1} is caused by the variation of the specific heat dependent on the reactants concentration. The hydrogen doping changes very little these properties. However, as can be seen in the results for $Y_{11} \sim 0.1$, the variation of the χ_f^{-1} is more important for the *n*-heptane doping in hydrogen flames.

From Fig. 7b, it is possible to note the variation of the flame temperature θ_f with mixture composition. By increasing the *n*-heptane mass fraction Y_{11}, the flame temperature decreases as a consequence of the increase in the radiative energy loss produced by the increase of the CO_2 concentration. An extra curve corresponding to the hydrogen mass fraction $Y_{21} = 0.02$ is presented in the flame temperature plot (Fig. 7b) in order to show the transition from the curve for $Y_{21} = 0.01$ to the curve for $Y_{21} = 0.03$. The curve for $Y_{21} = 0.01$ indicates a very small increase in the flame temperature as the *n*-heptane mass fraction is reduced. Also, a maximum value for θ_f is observed around $Y_{11} = 0.3$. Furthermore, the behaviour of the flame temperature in the range $0.3 < Y_{11} < 0.99$ shows that, although the total heat released decreases with the reduction of *n*-heptane in the mixture, the flame temperature increases because the radiative energy losses decreases slightly faster. The maximum flame temperature occurs when the reduction of the heat released is compensated integrally by the reduction of the radiative energy losses. By decreasing the *n*-heptane mass fraction further than $Y_{11} = 0.3$, the reduction in radiative energy losses is not enough to balance the reduction of the heat released, thereby the flame temperature decreases.

The curve for $Y_{21} = 0.02$ also shows maximum value for flame temperature about $Y_{11} = 0.1$. For the other two curves, $Y_{21} = 0.03$ and 0.05, the flame temperature increases continuously as the *n*-heptane is reduced in the mixture, showing that the heat released by the hydrogen reaction and the reduction of the radiative energy losses determine the flame temperature.

Hydrogen doping on the *n*-heptane diffusion flames ($Y_{11} \sim 1$) has effect on the flame temperature. However, the *n*-heptane doping on the hydrogen flames ($Y_{11} \sim 0.1$) produces a more significant modification on the flame temperature because it introduces in the gas phase the CO_2 that is main radiating species. Fig. 7c and d display the ratio d_2/d_1 and γ. As expected, the ratio d_2/d_1 presents a large variation in the range $0.1 < Y_{11} < 1.0$. Moreover, the variation augments with the increasing of the hydrogen mass fraction in the fuels mixture. The results for parameter γ, that can be used as an indication of the flame position inside the viscous layer, show a reduction of $-\gamma$ as the *n*-heptane concentration reduces. These two parameter will be used in future flame stability analyses.

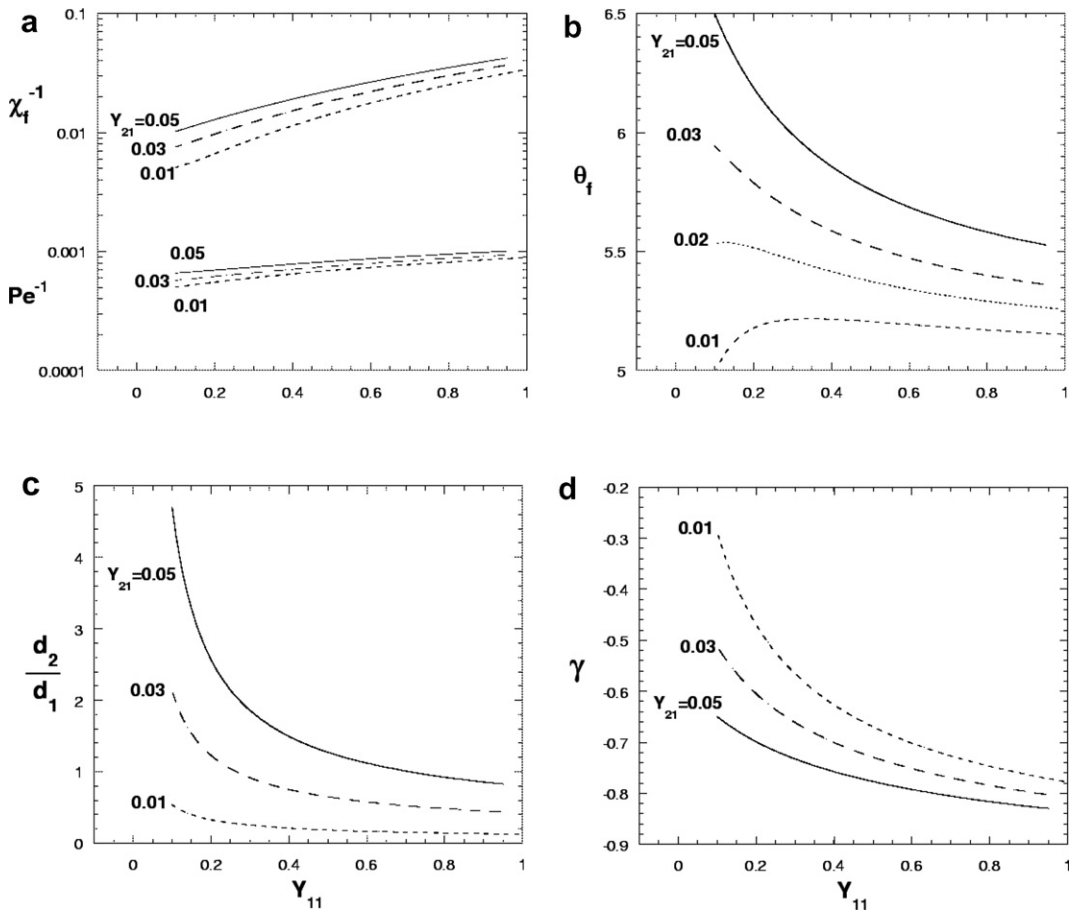

Fig. 7. Distribution of (a) the reciprocal scalar dissipation χ_f^{-1} and the reciprocal Peclet number Pe^{-1}; (b) flame temperature θ_f; (c) ratio d_2/d_1 and (d) the Liñán's parameter γ as a function of the *n*-heptane mass fraction Y_{11} for three the hydrogen mass fractions Y_{21}, 0.05, 0.03 and 0.01.

As in the other flame properties, the hydrogen doping ($Y_{11} \sim 1$) produces a modification on d_2/d_1 and γ, but the most significant modification is caused by the *n*-heptane doping ($Y_{11} \sim 0.1$).

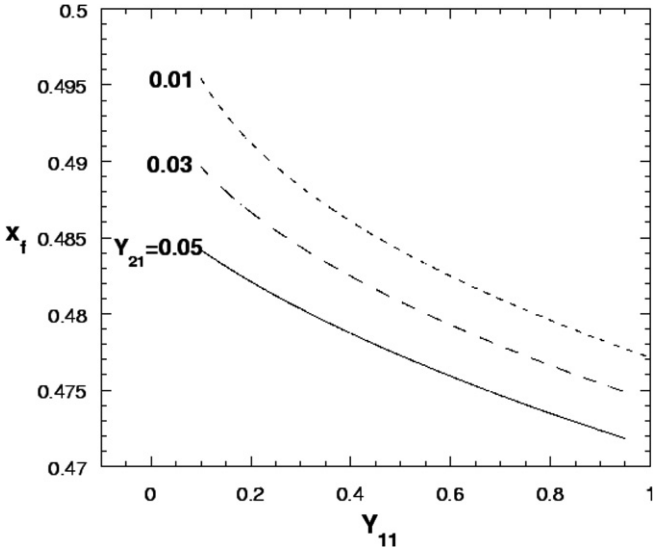

Fig. 8. Flame position x_f as a function of the *n*-heptane mass fraction Y_{11}. It is presented the flame position for three hydrogen mass fraction $Y_{21} = 0.01$, 0.03 and 0.05.

The dependence of the flame position x_f on the *n*-heptane mass fraction Y_{11} is illustrated in Fig. 8. To satisfy the stoichiometry, the flame takes place closer to the nozzle from where the oxygen stream comes out as higher is the fuel concentration in the mixture. As expected, this flame property does not exhibit difference between the hydrogen doping and *n*-heptane doping, indicating that flame position depends strongly on the total composition, not on the particular fuel composition in the conditions $Y_{11} \sim 0.1$ and $Y_{11} \sim 1$.

8. Comparison to simulation

In order to validate the extended Shvab–Zel'dovich formulation, a simulation is performed with the commercial reacting flow code ChemKin by assuming a *n*-heptane kinetic mechanism with 266 steps and 41 species [28]. Table 1 presents the results for the flame temperature θ_f and the flame position x_f determined by both simulations for four oxidant stream velocities, $v_0 = 0.5$, 1, 1.5 and 2 m/s. The maximum temperature obtained from the ChemKin code was compared to the data determined in this work. The

Table 1
Flame temperature θ_f and flame position x_f calculated considering infinite reaction rate and finite reaction rate

Oxidant stream velocities v_0 (cm/s)		50	100	150	200
Shvab–Zel'dovich model with infinite reaction rate	θ_f	5.9150	5.921	5.920	5.918
	x_f	0.4507	0.4647	0.4711	0.4749
ChemKin code with finite reaction rate [28]	θ_f	5.014	4.921	4.802	4.783
	x_f	0.4311	0.4598	0.4500	0.4630

composition of the fuel is such that $Y_{11} = 0.35$ and $Y_{21} = 0.05$. Since the reaction zone has a certain thickness when described by the aforementioned kinetic mechanism, it was difficult to specify the location in the flow field to determine the ratio d_2/d_1 and the parameter γ. Therefore, a comparison for these properties will be not presented.

As seen in Table 1, the results for the flame position x_f determined by both models show good agreement. This fact indicates that the flow field was reasonably described by the Shvab–Zel'dovich formulation despite all simplifications adopted in this work. Nevertheless, the results for the flame temperature are not so close, mainly for higher stream velocities. The discrepancy is related to the reaction rates, which are infinite in the simulation with Shvab–Zel'dovich model and finite in the Chemkin code. For a finite reaction rate, the residence time of the reactants inside the flame region decreases as the stream velocity increases. Thereby, an increase in the stream velocity leads to a reduction in the reaction rate, that causes a reduction in the flame temperature.

9. Conclusion

In this work, an extension of the Shvab–Zel'dovich formulation for diffusion flames is presented. The extended formulation has the advantage of working with conservation equations with smooth and distributed source terms instead of the Arrhenius exponential source. By assuming the Burke–Schumann kinetic mechanism, the extended Shvab–Zel'dovich formulation permits to study the properties of diffusion flames established by the burning of multicomponent fuels.

Calculations provided a qualitative information concerning the temperature, position and scalar dissipation of the *n*-heptane-hydrogen diffusion flame and the hydrogen doping *n*-heptane diffusion flames and *n*-heptane doping hydrogen diffusion flames. Since, in this model, the reaction rate was not affected by the flow field velocity, only the variation of the flame temperature by the radiative heat loss and the effective Lewis number could be studied. Also, the model brings to evidence the effects of the preferential hydrogen mass diffusion and the preferential *n*-heptane thermal diffusion on the flame.

Acknowledgements

The author acknowledges MSc Wilson de Freitas Muniz for performing the numerical calculation with the detailed *n*-heptane and hydrogen mechanisms. The author thanks the Reviewers for discussions of influences of preferential mass and thermal diffusions. This work was in part supported by the Conselho Nacional de Desenvolvimento Científico e Tecnológico – CNPq under the Grant 302801/03-0 and by Fundação de Amparo a Pesquisa do Estado de São Paulo – FAPESP under the Grant 00/08997-4.

References

[1] A. Hamins, K. Seshadri, The influence of alcohol on the combustion of hydrocarbon fuels in diffusion flames, Combust. Flame 64 (1986) 43–54.
[2] A. Hamins, K. Seshadri, The structure of diffusion flames burning pure, binary, and ternary solutions of methanol, heptane, and toluene, Combust. Flame 68 (1987) 295–307.
[3] A. Mukhopadhyay, D. Sanyal, A study of thin-flame quasisteady sphericosymmetric combustion of multicomponent fuel droplets. part i: Modelling for droplet surface regression and non-unity gas-phase lewis number, Int. J. Energy Res. 23 (1999) 963–977.
[4] A. Mukhopadhyay, D. Sanyal, A study of thin-flame quasisteady sphericosymmetric combustion of multicomponent fuel droplets. part ii: Parametric studies, Int. J. Energy Res. 23 (1999) 979–987.
[5] A. Mukhopadhyay, D. Sanyal, A parametric study of burning of multicomponent droplets in a dilute spray, Int. J. Energy Res. 25 (2001) 1295–1314.
[6] F.F. Fachini, Large-activation-energy asymptotic analysis of multicomponent fuel diffusion flames, Combust. Sci. Technol. 177 (2005) 1793–1811.
[7] F.F. Fachini, Multicomponent fuel diffusion flames: flame structure for coupled diffusion-flame and premixed-flame burning regimes, in: 43rd AIAA Aerospace Sciences Meeting and Exhibit (2005), AIAA Paper 2005-0550, Reno NV, January 10–13, 2005.
[8] A. Liñán, The structure of diffusion flames, in: Fluid Dynamical Aspects of Combustion Theory, Longman Scientific and Technical (Pitman Research Notes in Mathematics, No. 223), Harlow, UK, 1991, pp. 11–29.
[9] A. Liñán, Diffusion-controlled combustion, in: H. Aref, J.W. Philips (Eds.), Mechanics for a New Millenium, Kluwer Academic Publishers, Netherlands, 2001, pp. 487–502.
[10] A. Liñán, F.A. Williams, Fundamental Aspects of Combustion, Oxford University Press, Oxford, UK, 1993.
[11] F.F. Fachini, A. Liñán, F.A. Williams, Theory of flame histories in droplet combustion at small stoichiometric fuel–air ratios, AIAA J. 37 (1999) 1426–1435.
[12] J.M. Prausnitz, Molecular Thermodynamics of Fluid–Phase Equilibria, Prentice-Hall, Inc., Englewood Cliffs, NJ, 1969.
[13] S.H. Lam, J. Bellan, On de-coupling of shvab-zel'dovich variables in a presence of diffusion, Combust. Flame 132 (2003) 691–696.
[14] Y. Tambour, B. Gal-Or, Phenomenological theory of thermodynamic coupling in multicomponent compressible laminar boundary layers, Phys. Fluids 19 (1976) 219–226.
[15] S.P. Burke, T.E.W. Schumann, Diffusion flames, Ind. Eng. Chem. 20 (1928) 998–1009.
[16] M. Sibulkin, S. Malary, Diffusion flame calculations for nonunity lewis number, Combust. Sci. Technol. 28 (1982) 85–88.
[17] T. Takagi, Z. Xu, Numerical analysis of laminar diffusion flames – effects of preferential diffusion of heat and species, Combust. Flame 96 (1994) 50–59.
[18] C.K. Law, S.H. Chung, Steady diffusion flame structure with Lewis number variations, Combust. Sci. Technol. 29 (1982) 129–145.

[19] C.E. Frozakis, A.G. Tomboulides, P. Papas, P.F. Fisher, R.M. Rais, P.A. Monkewitz, K. Boulouchos, Three-dimensional numerical simulations of cellular jet diffusion flames, Proc. Combust. Inst. 30 (2005) 185–192.
[20] J.S. Kim, V. Gubernov, On the fast-time cellular instabilities of liñán's diffusion-flame regime, Combust. Sci. Technol. 177 (2005) 991–1022.
[21] H. Tsuji, Counterflow diffusion flames, Prog. Energy Combust. Sci. 8 (1982) 93–119.
[22] G.L. Hubbard, C.L. Tien, Infrared mean absorption coefficients of luminous flames and smoke, J. Heat Transfer 100 (1978) 235–239.
[23] M.L. Rightley, F.A. Williams, Structures of co-diffusion flames near extinction, Combust. Sci. Technol. 125 (1997) 181–200.
[24] A. Liñán, El Papel de la Mecánica de Fluidos en los Processos de Combustión, Real Academia de Ciencias Fisicas y Naturales, Madrid, Spain, 1991.
[25] F.F. Fachini, An analytical solution for the quasi-steady droplet combustion, Combust. Flame 116 (1999) 302–306.
[26] A. Liñán, The asymptotic structure of counterflow diffusion flame for large activation energy, Acta Astronaut. 1 (1974) 1007–1039.
[27] N. Peters, Laminar diffusion flamelet models in non-premixed turbulent combustion, Prog. Energy Combust. Sci. 10 (1984) 319–339.
[28] T.J. Held, A.J. Marchese, F. Dryer, A semi-empirical reaction mechanism for *n*-heptane oxidation and pyrolysis, Combust. Sci. Technol. 123 (1997) 107–146.